North Atlantic MOC variability and the Mediterranean Outflow: a box-model study

By SANDRO CALMANTI[1]*, VINCENZO ARTALE[1] and ALFONSO SUTERA[2], [1]*Ente per le Nuove tecnologie, l'Energia e l'Ambiente, Rome, Italy;* [2]*University La Sapienza, Rome, Italy*

ABSTRACT

A simple box-model is used to investigate the effect of intermediate level heat/freshwater fluxes on the variability of the oceanic meridional overturning circulation. The model includes a simple representation of the spreading of the Mediterranean Outflow Water in the North Atlantic. We identify an *internal* advective feedback affecting the amplitude of the thermohaline oscillations. When a salinity gradient is maintained in the ocean interior the oscillations are amplified. Instead, if the intermediate level fluxes are spread in the ocean deep layers, the model variability is reduced. We suggest that this mechanism may be relevant for climate variability on interdecadal timescales.

1. Introduction

A broad spectral peak at frequencies ranging from 10 to 50 yr is a distinctive feature of the climate variability observed over the North Atlantic (Marshall et al., 2001). Such a spectral peak is loosely attributed to the effect of thermohaline processes in the ocean. In fact, a common feature of ocean-atmosphere general circulation models (OAGCMs) is the occurrence of interdecadal variability of the meridional overturning circulation (MOC) and of the associated transport of heat and freshwater (Delworth et al., 1993; Weisse et al., 1994). However, the large number of parameters involved in their formulation make GCM's experiments a rather uncomfortable tool for detecting well-defined cause-effect relations. Instead, Stommel-type box-models (Stommel, 1961) have been extensively used as powerful conceptual tools to investigate feedbacks and instabilities of the MOC and to explain the possibility of observing more than one equilibrium in the circulation of the global ocean (Cessi, 1994; Rahmstorf, 1996; Scott et al., 1999; Lucarini and Stone, 2005). Another useful application of such simple models is the analysis of the mechanisms affecting the variability of heat and mass transport in the ocean at interdecadal timescales. For example, Griffies and Tziperman (1995) explained the MOC variability obtained by Delworth et al. (1993) in terms of the stochastic excitation of a damped linear oscillatory eigen-mode of the system. They interpreted the stochastic forcing as the effect of high-frequency atmospheric variability, de-correlated with the oceanic behavior.

An alternative explanation was given by Rivin and Tziperman (1997) who introduced, in the same Stommel-type box-model, an ad hoc saturation mechanism producing self-sustained oscillation with no need for random input of energy from the atmosphere. However, adopting a purely statistical approach, they where not able to identify a definite role of non-linear processes in the description of the variability of coupled OAGCM experiments such as the one of Delworth et al. (1993).

In this paper, we consider a specific mechanism affecting MOC variability: the spreading of Mediterranean Outflow Water (MOW) in the North Atlantic. We focus on linear dynamics only. However, by considering different scenarios for the spreading of MOW, we seek to contribute to the understanding of the mechanisms producing the characteristic spectral peak of climate variability at interdecadal time-scale. We employ for our study a Stommel-type box-model similar to that of Tziperman et al. (1994). We extend their model by including an additional forcing which is aimed at representing the spreading of the MOW in the North Atlantic.

The Mediterranean Outflow can be considered as a mapping into the interior of the North Atlantic of the net evaporation and heat exchange occurring inside the Mediterranean basin. Quantitatively, it is a major contributor to the freshwater budget of the North Atlantic (Curry et al., 2003). In particular, about 1 Sv of Mediterranean Outflow, 1 psu saltier than the Atlantic inflow in the Mediterranean, corresponds to about 10–20% of the net annual evaporation over the North Atlantic (Gerdes et al., 1999). However, there is substantial uncertainty concerning the path of MOW in the North Atlantic (Bower et al., 2002; Sparrow et al., 2002) and its impact deep water formation occurring in the North Atlantic (Reid, 1979; McCartney and Mauritzen, 2001). Here,

*Corresponding author.
e-mail: sandro.calmanti@casaccia.enea.it

we compare two substantially different scenarios: in one case, we assume that the outflow mixes with newly formed deep waters at high latitudes before having any other interaction with the overlying atmosphere; in the other case, we assume that MOW is carried to the oceanic surface layers by the average large-scale circulation and is allowed to exchange heat and freshwater with the overlying atmosphere before entering the regions of deep water formation. The role of the intermediate level anomaly on the oscillatory behavior will be examined in the presence of a surface stochastic forcing.

The paper is organized as follows: in Section 2 we discuss the model equations; in Section 3 we discuss the equilibria of the model in the presence of intermediate depth anomalies and summarize some results concerning the linear stability analysis of the system; the effect of a stochastic surface forcing is examined in Section 4; discussion and conclusions are left to Section 5.

2. Model description

This study will focus on the damped linear oscillatory eigenmode of the MOC appearing in pure thermohaline models. The oscillation, which is described in details by Griffies and Tziperman (1995), can be summarized as follows. We assume that the strength of the MOC in a thermally direct equilibrium is regulated only by the meridional density gradient resulting from the heat/freshwater exchanges with the atmosphere and by the heat/freshwater transport in the ocean. A freshening of the oceanic surface layers in the cold, deep water formation regions reduces the meridional density gradient, thereby weakening the overturning. The weak overturning favors a longer residence time of surface waters in the evaporative regions at low latitudes. There, the salt content is increased. Eventually, these water masses are advected poleward so that the meridional pressure gradient increases and the overturning strengthens. A strong overturning implies less residence time in evaporative regions: fresher water masses are transported to high latitudes and the cycle starts over again. The heat transport has opposite effect on density and contributes to damp the oscillations. However, if the amplitude of the freshwater forcing is large enough, the oscillations may become unstable.

Such oscillatory mechanism originates from two key features of the large-scale ocean circulation that can be easily included in a simplified model of the MOC. The first is some functional dependence of the meridional overturning on the meridional density gradient, which follows from simple scaling arguments based on geostrophic assumptions (see Welander, 1971). The second feature is the dynamical separation of heat and freshwater fluxes in the buoyancy forcing, accounting for the different mechanisms driving the exchanges of heat and freshwater between the ocean and the atmosphere (Mikolajewicz and Maier-Reimer, 1994). Here, we use a box-model similar to the one of (Tziperman et al., 1994) which satisfies the two above-mentioned requirements. However, we include also a simple description of
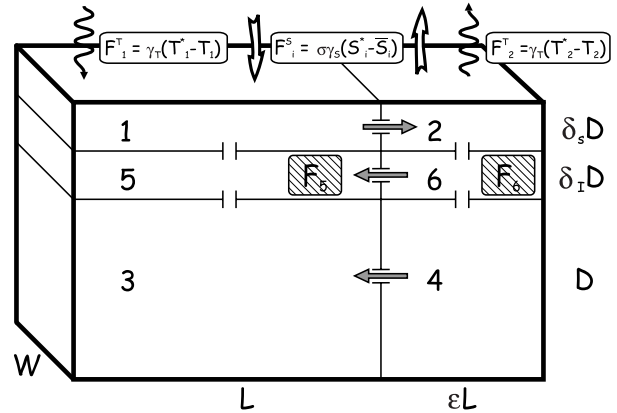

Fig. 1. Box-numbering and model scenarios. The forcing terms F_1 and F_2 in eqs. (A5) and (A6) are reported in the white boxes; the steady state values $\overline{S}_i$ are computed in a spinup integration during which the surface salinity is relaxed to climatology. The dashed box represents the additional internal forcing for the scenarios $M5$ and $M6$. The model parameters are: $V = D \cdot L \cdot W = 8.0 \, 10^{16} \, \mathrm{m}^3$; $\delta_I = 0.05$; $\delta_S = 0.05$; $\epsilon = 0.1$; $T_1^* = 25.0 \,^\circ \mathrm{C}$; $T_2^* = 0.0 \,^\circ \mathrm{C}$; $\gamma_T = 1/90$ days; $\gamma_S = \gamma_T/4$. To compute the values $\overline{S}_i$, we use $S_1^* = 36.5 \, \mathrm{psu}$ and $S_2^* = 34.5 \, \mathrm{psu}$ during the spinup. A linear equation of state is employed with thermal and haline expansion coefficients set to $\alpha = 1.6 \cdot 10^{-4} \,^\circ \mathrm{C}^{-1}$ and $\beta = 7.6 \cdot 10^{-4} \, \mathrm{psu}^{-1}$, respectively. The parameter σ is used as control parameter for the bifurcation analysis. The arrows represent the basic state circulation around which linear dynamics is investigated.

the MOW by adding, between the surface and the deep boxes, an intermediate layer that can be subject to additional heat and freshwater forcing. A sketch of the model configuration, along with a description of the symbols used throughout the paper, is shown in Fig. 1. The derivation model equations is presented in Appendix A.

2.1. Internal anomalies

To account for the presence of MOW in the North Atlantic, we introduce additional heat and freshwater fluxes in the intermediate level boxes. Three different scenarios of the model are compared. In the standard scenario, called $M0$, the model is only subject to surface heat and freshwater forcing. This model scenario can be compared to the equivalent 4-box formulation of Griffies and Tziperman (1995) by collapsing the intermediate boxes on the deep boxes. In particular, the oscillatory mechanism described at the beginning of Section 2 evolves in the same way, both in the 4-box formulation and in our scenario $M0$.

In the scenario $M5$, the additional forcing is imposed to box 5. In order to represent the characteristics of the Mediterranean Outflow, we assume that an outflow of 1 Sv at about 1 psu higher than Atlantic waters at the same depth is uniformly distributed over the whole volume of box 5. Therefore, the internal salinity forcing F^S_5 is taken as:

$$F_5^S = \frac{\Delta S \, \Phi_{Med}}{\delta_I \, V}, \tag{1}$$

where $\Delta S = 1$ psu, $\Phi_{\mathrm{Med}} = 1$ Sv $\equiv 10^6$ m^3 s^{-1} and the factor $\delta_I V$ accounts for the volume of box 5. The salt flux is balanced by a corresponding heat flux, $F_5^T = \frac{\beta}{\alpha} F_5^S$, such that, assuming a linear equation of state, density is not directly affected by the additional forcing. Notice that the compensation between temperature and salinity anomalies is observed in the real ocean, where recent changes of the bulk temperature and salinity of the outflow water have left density almost unchanged (Potter and Lozier, 2004).

To avoid the net accumulation of salt, owing to the presence of the additional internal flux, an adjustment F_i' ($i = 1, 2$) must be added to the surface freshwater flux such that:

$$\begin{cases} F_1' = F_2', \\ \delta_S F_1' + \delta_S \epsilon F_2' = -\delta_I F_5^S. \end{cases} \tag{2}$$

With this adjustment to the surface forcing, the meridional density gradient is not affected because the corrections F_1' and F_2' are equal (first of eq. 2). Yet, the salt content is conserved because the additional amount of salt extracted from box 1 and box 2 equals the amount of salt injected in box 5 (second of eq. 2). From eq. (2) we have that the adjustment of the surface freshwater fluxes must be implemented in the model equation for the scenario $M5$ by operating the following substitution:

$$F_i \rightarrow F_i + F_i' = F_i - \frac{\delta_I F_5^S}{\delta_S(1 + \epsilon)}. \tag{3}$$

No such adjustment is required for the heat content, because the surface temperature is restored to climatological values.

Analogous changes are applied for the scenario $M6$, where the intermediate level forcing is applied to the box 6, except that:

$$F_6^S = \frac{\Delta S \, \Phi_{\mathrm{Med}}}{\delta_I \epsilon \, V}, \tag{4}$$

and

$$F_i \rightarrow F_i + F_i' = F_i - \frac{\delta_I \epsilon \, F_6^S}{\delta_S(1 + \epsilon)}. \tag{5}$$

The weighting factors in the denominator of eqs. (1) and (4) account for the spreading of the same amount of salty water over boxes having different volume. Physically, the scenario $M5$ represents the scenario in which MOW is carried to the oceanic surface layers by the basic state circulation and heat/freshwater exchanges occur in some unspecified region of the North Atlantic, outside the deep water formation region; in the scenario $M6$ the mixing of MOW with newly formed deep waters occurs at high latitudes, before any other interaction with the overlying atmosphere.

3. Steady states

Since a thorough exploration of the various model parameters shows that, when the thermal forcing is sufficiently strong, the circulation regime sketched in Fig. 1 is a general occurrence of the box-model under study, we skip the complete discussion of the model sensitivity to the various parameters. Instead, we

choose a parameter set-up which is tuned to produce a strength of the circulation that can be considered as descriptive of the real ocean. However, we stress that the results presented below do not follow from quantitative details such as those concerning the geometric set-up and the corresponding strength of the overturning. Rather, the physical processes described below are characteristic of the linear oscillations around the steady state sketched Fig. 1.

To illustrate the general stability properties of such circulation regime, we allow the amplitude of the surface freshwater forcing—the parameter σ shown in Fig. 1—to vary over an interval which is large enough to span different stability regimes. The parameter σ is introduced by first integrating the model equations to equilibrium with the surface salinity relaxed to a given climatology. Then, the values of surface salinity obtained at equilibrium, are employed to compute the standard value of the surface freshwater flux which corresponds to $\sigma = 1$ (see Fig. 1 for more details). The maximum descent method (Press et al., 2001) was employed to compute the bifurcation diagram of the system for the three model scenarios $M0$, $M5$ and $M6$, with σ as control parameter. The structure of the bifurcation diagram is basically the same as in Tziperman et al. (1994), so we briefly summarize only those features which are relevant to our analysis.

For small values of σ, two steady solutions exist. The solution corresponding to the strongest overturning is stable, whereas the weak overturning corresponds to unstable solutions. As σ grows, a linear oscillatory eigenmode appears on the stable branch of solutions. The physical mechanism for the oscillation is the one described at the beginning of Section 2. A critical value σ_c exists, after which the oscillatory mode becomes unstable and the branch of solutions connects with the unstable branch characterized by small values of the overturning. The dynamics of small perturbations around this branch of solution is shown in Fig. 2 by reporting the real and imaginary components of the eigenvalues associated with the most unstable eigenmode of the linearized system. The three model scenarios, $M0$, $M5$ and $M6$ are destabilized in correspondence with slightly different values of σ_c:

$$M0 \rightarrow \sigma_c = 1.21,$$

$$M5 \rightarrow \sigma_c = 1.15,$$

$$M6 \rightarrow \sigma_c = 1.23.$$

In the stable regime, the relative magnitude of the real part of the eigenvalues at fixed values of σ represents the decaying rate of the oscillatory eigenmode. Therefore, at fixed σ, the scenario $M5$ is the less damped (Fig. 2) and small initial perturbation to an equilibrium of $M5$ results into more persistent oscillations than in the other two cases. Instead, the scenario $M6$ is the most stable. A thorough discussion of the stabilizing and destabilizing feedback for the three model scenarios is presented in Section 4.2.
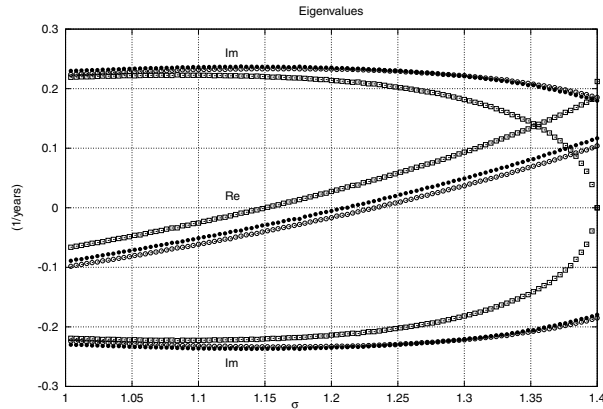
Fig. 2. Real and imaginary parts of the eigenvalues corresponding to the first unstable eigenmode on the branch of stable solutions. Eigenvalues are shown for the three model scenarios: M0 (solid points); $M5$ (hollow squares); M6 (hollow points). See Section 2.1 for a definition of the model scenarios.

A first insight into the different behavior of the three model scenarios can be gained by discussing the equilibrium solution at a particular value of the control parameter where all model scenarios are stable (Fig. 3).

With the circulation pattern sketched in Fig. 1, in the absence of internal forcing (scenario $M0$), all values of temperature and salinity in the intermediate and deep layers must be equal to those in box 2 (Fig. 3a). The strength of the overturning at equilibrium is determined by the density difference between the surface boxes (see eqs. A2–A4).

In the scenario $M5$ (Fig. 3b), the impact of the internal forcing on temperature is weak. In fact, since surface temperatures are restored to 'climatological' values, the heat carried to the surface layer is promptly released to the atmosphere within the northward traveling branch of the overturning. Thus the water mass which is cooled at high latitudes contributes to the cooling of the intermediate level water in the equatorial box. Therefore, the temperature of box 5, whose increase could be expected to meet the density compensation constrain imposed to the intermediate level forcing, remains close to the temperature of the other subsurface boxes. As an example, we note that in Fig. 3b, the difference between the temperature of box 5 and the temperature of

the other deep and intermediate level boxes is around 0.015 °C, which is not density-compensating for the corresponding salinity difference of about 0.06 psu. In fact, the dissipation of salinity anomalies is not permitted, because the freshwater flux applied at the surface is steady. Thus, substantial salinity gradient can be maintained in the intermediate layer. The composition of the temperature anomaly and of the salinity anomaly in box 5 results into a net density gradient in the intermediate layer, which is not present in the other scenarios and is not imposed directly with the introduction of the additional forcing. The effect of the density gradient in the intermediate layer is to reduce the strength of the meridional overturning in the scenario $M5$.

In the scenario $M6$ (Fig. 3c), a vertical salinity gradient appears between box 2 and box 6. Notice that the internal forcing is introduced as a positive input of heat and salt in box 6. However, because of the constrain to the total salt content, the introduction of the intermediate level positive salt flux appears as a freshening of the surface layer, compared to the scenarios $M0$ and $M5$. In the scenario $M6$, the heat and salt anomalies are spread to the other subsurface boxes and the intermediate and deep meridional temperature and salinity gradients are not affected by the presence of the intermediate level forcing. Therefore, as in the scenario $M0$, the strength of the overturning is controlled only by the density difference of the surface boxes.

The main point of the above discussion is that in the scenarios $M0$ and $M6$, the flow is controlled only by the heat and salt content of the surface boxes. Instead, in the scenario $M5$ a salinity gradient is maintained in the ocean interior. It contributes to determine the strength of the overturning and plays an important role in the presence of oscillations, as described in the next section.

4. Stochastically forced oscillation

As suggested by Griffies and Tziperman (1995) and Rivin and Tziperman (1997) the excitation of an oceanic damped oscillatory eigenmode by means of stochastic surface forcing, may explain the dynamics of the low-frequency (interdecadal) variability observed in the coupled OAGCM simulation of Delworth et al. (1993). A further support to this hypothesis comes from the work of Weisse et al. (1994) who analyzed the Principal

Fig. 3. Model equilibria on the stable branch for the three model scenarios: $M0$ (a); $M5$ (b); $M6$ (c). Temperature values are shown for each box in plain font, in the left and right columns of each box, with the same ordering as in Fig. 1. Salinities are indicated in italic fonts. The central column of each box indicates the transport in the surface, intermediate and deep layer. All equilibria are computed for $\sigma = 1.1$. Units are ° C for temperature, psu for salinity and Sverdrup ($1\,\mathrm{Sv} \equiv 10^6\,\mathrm{m}^3\,\mathrm{s}^{-1}$) for transport.

(a)		
24.393 *36.550*	**17.03**	6.069 *35.377*
6.069 *35.377*	**-0.81**	6.069 *35.377*
6.069 *35.377*	**-16.22**	6.069 *35.377*

(b)		
24.413 *36.605*	**16.28**	5.870 *35.372*
5.884 *35.433*	**-1.12**	5.870 *35.372*
5.870 *35.372*	**-15.16**	5.870 *35.372*

(c)		
24.393 *36.501*	**17.00**	6.060 *35.320*
6.061 *35.379*	**-0.80**	6.061 *35.379*
6.061 *35.379*	**-16.20**	6.061 *35.379*
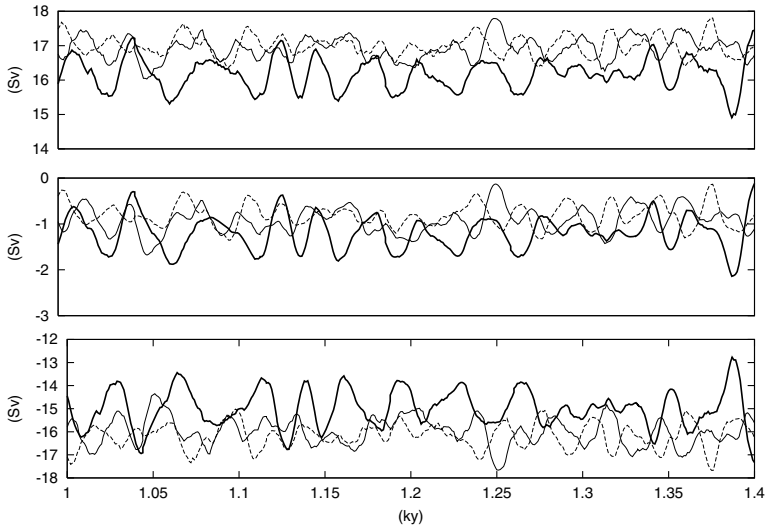
Oscillation Patterns of an OGCM with realistic topography. They showed that the occasional freshening of the Labrador Sea due to a stochastic component of the freshwater flux, and the successive freshening of the North Atlantic causes the fluctuations of the meridional overturning circulation and of the corresponding heat transport. Building on this hypothesis, we modify the surface freshwater forcing by substituting the eqs. (A5) and (A6) for the salt content with:

$$\dot{S}_1 = \frac{U_{1-2}}{V}(S_5 - S_1) + \gamma_S\left(S_1^* - \overline{S}_1\right) + w_1\xi, \tag{6}$$

$$\dot{S}_2 = \frac{U_{1-2}}{\epsilon V}(S_1 - S_2) + \gamma_S\left(S_2^* - \overline{S}_2\right) + w_2\xi, \tag{7}$$

where w_1 and w_2 are two independent Wiener processes and ξ is the amplitude of the stochastic component of the surface freshwater forcing. We took ξ such that the stochastic component of the surface forcing has a variance corresponding to 10% of the steady component.

4.1. Flow dynamics

In Fig. 4, we compare a sample of the oscillations obtained at $\sigma = 1.1$, where all three model scenarios are linearly stable.

As expected from the linear stability analysis, the period of the oscillation derived from the imaginary part of the complex eigenvalue—$T = 2\pi/\lambda_{Im}$—is about 30 yr for all of the model scenarios. The northward flow is always carried in the surface layer, whereas the return southward flow is carried in the intermediate and deep layers.

It is interesting to observe that the anomalous flow have the same sign in the surface layer and in the intermediate layer. Such a dynamics of the anomalous flow is equivalent to the one that can be generated by applying the corresponding pressure differences in a system of connected pipes and carries important informations as to how anomalous flows are generated in such a simple model. In fact, as indicated in eqs. (A2)–(A4), if a density
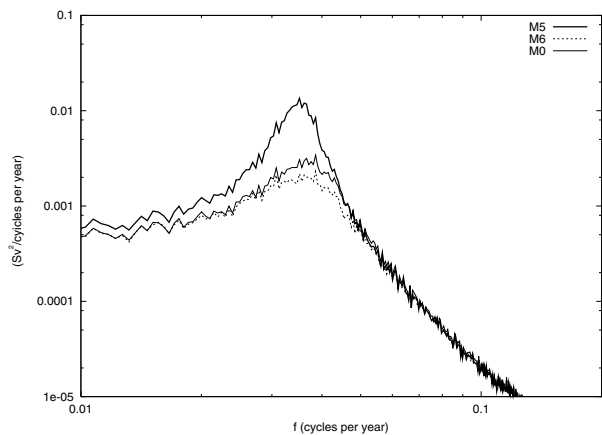
gradient is applied only in the surface layer, an anomalous flow is generated in the intermediate and in the deep layer against the corresponding pressure gradient. By continuity, this flow is balanced with a return flow in the surface layer. Instead, if the density gradient is in the intermediate or in the deep layer, the flow against the pressure gradient involves only the deep layer and the return flow is in the surface layer and in the intermediate layer. Therefore, the flow dynamics reported in Fig. 4 implies that the overturning fluctuations are dominated by anomalous density gradients in the deep boxes. In particular, we found that the correlation between the anomalous flow and the anomalous density gradient between box 3 and box 4 is about $r = 0.8$. Instead, the anomalous gradients in the surface layer and in the intermediate layer are de-correlated with the anomalous flow.

A more quantitative view of the differences between the three scenarios is given in Fig. 5 by comparing the average power spectrums over 100 different integrations of the model equations for

Fig. 6. Anomalous overturning U_{1-2} (abscissa) versus the term $-U'_{3-4}(\overline{S}_3 - \overline{S}_5)/(\delta_I V)$, representing the salinity trend in box 5 due to the anomalous transport of the basic state salinity gradient (ordinates).

Fig. 7. Anomalous overturning U_{1-2} (abscissa) versus the term $U'_{1-2}\,\delta_S(\overline{S}_2 - \overline{S}_6)/(\delta_I \epsilon V)$ representing the salinity trend in box 6 due to the anomalous transport of the basic state salinity gradient (ordinates).
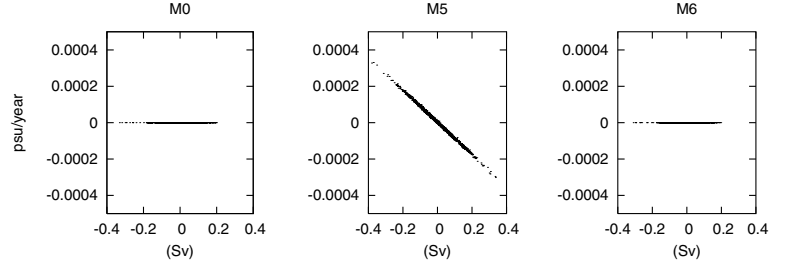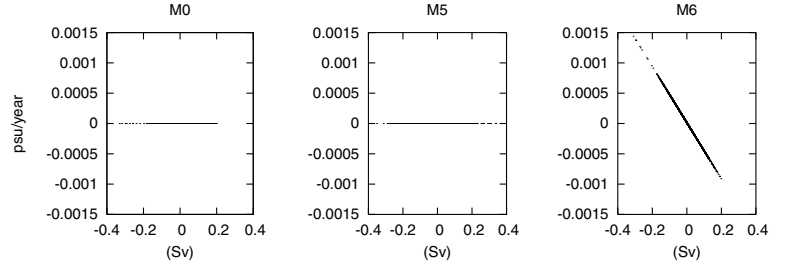
the three scenarios with stochastic surface forcing. The position of the peaks differ slightly, with the scenario $M5$ oscillating at slower frequencies than the scenarios $M0$ and $M6$. Physically, this is a direct consequence of the decreased overturning of $M5$ (Fig. 3b). The spectrums differ substantially in the height of their peaks, with the scenario $M5$ having higher energy on the characteristic timescale of the linear advective oscillation. Instead, a slight damping is observed in the case of the scenario $M6$ with respect to the scenario $M0$.

4.2. The linearized system

To identify the physical mechanism which is responsible for the different behavior of the three model scenarios, we systematically looked at the evolution of each component of the model equations during the course of the oscillations. In particular, since the response of the system to the applied stochastic forcing is that of a damped linear oscillator, it is instructive to focus on linear dynamics by decomposing each contribution to the tendency of heat and salinity as:

$$\overline{U}\,\Delta C' + U'\,\Delta\overline{C}, \tag{8}$$

where over-lined quantities are characteristic of the steady states, and primed quantities represent perturbations. In eq. (8) we separate the contribution of the basic state advection of the anomalous gradients (first term) from the anomalous advection of the steady state gradients (second term).

Given the structure of the equilibria discussed in Section 3 (Fig. 3), we expect, in the scenario $M5$, a relevant role of the terms $U'\,\Delta\overline{S}$ affecting the freshwater budget of the intermediate layer. In Fig. 6, we show a scatter plot of the anomalous overturning (i.e. the term U'_{1-2} resulting from the decomposition $U_{1-2} = \overline{U}_{1-2} + U'_{1-2}$), versus the anomalous advection of

the mean salinity gradient, i.e. the term $-U'_{3-4}\,(\overline{S}_3 - \overline{S}_5)/(\delta_I V)$ which appears in the linearized version of eq. (A9). The negative correlation in the scenario $M5$ indicates a positive feedback between the anomalous overturning and the anomalous advection of salt in the deep layers. In fact, as the circulation strengthens, fresher water masses are advected from the polar to the equatorial boxes. The freshening of intermediate waters at low latitude amplifies the meridional density gradients and the overturning circulation is further strengthened. This feedback is responsible for the strong peak of variability in the power spectrum shown in Fig. 5: it cannot exist in the other scenarios because in those cases the intermediate and deep level salinity gradient vanishes. Accordingly, in Fig. 6, the anomalous advection of the basic state salinity gradient vanishes for the scenarios $M0$ and $M6$.

Similar arguments explain the increased stability, and therefore the reduced variability, which is observed in the scenario $M6$. In Fig. 7, we show a scatter plot of the term $U'_{1-2}\,\delta_S\,(\overline{S}_2 - \overline{S}_6)/(\delta_I \epsilon V)$ appearing in the linearized equation for S_6 versus the anomalous overturning U'_{1-2}. In this case, when the overturning increases, more freshwater is carried from box 2 to box 6. As a consequence, the effect of the intermediate level salt flux anomaly is partially reduced—the salinity of box 6 decreases—and the meridional density and pressure gradients are also reduced. Therefore, the presence of a salinity difference between box 2 and box 6—which is caused by the presence of the intermediate level forcing—produces a negative feedback on the amplitude of the overturning fluctuations. This effect increases the stability of the scenario $M6$ and reduces the amplitude of variability as shown in the power spectrum in Fig. 5. Such mechanism is not allowed in the other model scenarios where $\overline{S}_2 - \overline{S}_6 = 0$.

To summarize, we have demonstrated that the presence of an intermediate level forcing has a stabilizing effect in the

scenario $M6$, when the anomalous salt flux is injected in the intermediate layer and spreads directly in the deep ocean. Instead, in the scenario $M5$, where the anomalous salt flux is injected in the intermediate layer and carried to the surface by the mean flow, the intermediate level forcing has a destabilizing effect and amplifies the characteristic linear oscillations at interdecadal timescale.

5. Conclusions

In this paper, we have analyzed the variability of a simple box-model of the oceanic meridional overturning circulation in the presence of intermediate level heat/freshwater forcing, representing the spreading of MOW in the North Atlantic. We have analyzed three different scenarios of the system. The instabilities of the standard case $M0$ (without internal forcing) are identical to those described by Tziperman et al. (1994) in a similar box-model study. The relevance of such instabilities to the interpretation of variability in coupled GCM's simulations is discussed by Griffies and Tziperman (1995). Here, we have shown that internal forcing may affect the system in two substantially different ways.

One possibility (scenario $M6$) is that the internal anomaly directly mixes with newly formed deep waters. In this case the efficiency of oscillatory mechanism is reduced, the oscillations are damped and the internal anomaly turns out to be a stabilizing factor.

A second possibility (scenario $M5$) is that the intermediate level anomaly affects the processes of deep-water formation only after having interacted both with other water masses produced in the system and with the atmosphere. In this case, the presence of an intermediate level forcing, acts as a destabilizing factor for the convective system. In the presence of stochastic atmospheric forcing, the scenario $M5$ shows a significantly higher peak of variability at frequencies which are characteristic of the linear thermohaline oscillations. We attribute such an enhanced variability to the presence of a positive internal advective feedback, which is permitted by the maintenance of a salinity gradient in the ocean interior.

In the past, a few authors have addressed, in the context of GCMs studies, the question of the impact of MOW on the North Atlantic MOC (Chan and Motoi, 2003; Artale et al., 2002; Rahmstorf, 1998). All these studies demonstrate that the impact on the strength of the overturning is indeed marginal. However, we have shown here that another qualitatively important impact of MOW is on the variability of the overturning. To our knowledge, no such sensitivity study on GCMs has been performed to date. Therefore, we suggest that the design and analysis of suitable GCM simulation has an important subject for future studies. In particular, sensitivity studies involving the spreading of MOW in the North Atlantic may help distinguishing between linear and non-linear process in sustaining interdecadal oceanic variability, in the sense discussed by Rivin and Tziperman (1997). In fact, we

have shown that under certain condition related to the spreading of MOW in the North Atlantic (our scenario $M5$), linear dynamics alone is sufficient to explain the presence of a strong spectral peak in the variability of the MOC at interdecadal timescale. Instead, other spreading scenarios (such as our scenario $M6$) would require additional energy input and/or alternative mechanism to explain the same spectral peak. The diagnostics employed in this work to identify the feedbacks between the strength of the overturning circulation and the anomalous transport in the intermediate layers, can be easily applied to the output of coupled GCM's simulation. Thus, it can be a useful tool to check whether the mechanism described in this paper have a significant role in the real ocean.

6. Acknowledgments

7. Appendix A

The model geometry and box numbering is shown in Fig. 1. The model equation can be formally derived by discretizing the same two-dimensional convection equation as in Tziperman et al. (1994). To derive the meridional pressure gradient, the hydrostatic pressure is computed at the center of each box, by vertically integrating the equation of state, which is assumed to be linear. In doing so, an undetermined constant representing the surface pressure appears. This is eliminated by imposing that the vertically integrated meridional transport is zero:

$$U_{1-2} + U_{5-6} + U_{3-4} = 0. \tag{A1}$$

After some algebra, we obtain:

$$\begin{aligned} U_{1-2} = \delta_S\,\overline{U}_0\,[(\rho_4 - \rho_3) + (\rho_6 - \rho_5)(2 + \delta_I)\delta_I \\ + (\rho_2 - \rho_1)(1 + \delta_I)\delta_S], \end{aligned} \tag{A2}$$

$$\begin{aligned} U_{3-4} = \overline{U}_0\big[-(\rho_4 - \rho_3)(\delta_I + \delta_S) + \\ - (\rho_6 - \rho_5)(\delta_I + 2\delta_S)\delta_I - (\rho_2 - \rho_1)\delta_S^2\big], \end{aligned} \tag{A3}$$

$$\begin{aligned} U_{5-6} = \delta_I\,\overline{U}_0\,\big[(\rho_4 - \rho_3) + (\rho_6 - \rho_5)(1 - \delta_S)\delta_I + \\ - (\rho_2 - \rho_1)\delta_S^2\big]. \end{aligned} \tag{A4}$$

An upwind differencing scheme is used to compute the transport of tracers between the boxes. The advection of heat and salt is evaluated by taking into account the origin of the water mass which is advected in each box. The overturning circulation qualitatively depicted in Fig. 1 is described by the following set of

equations for the evolution of temperature and salinity in each box:

$$\dot{C}_1 = \frac{U_{1-2}}{V}(C_5 - C_1) + F_1,$$ (A5)

$$\dot{C}_2 = \frac{U_{1-2}}{\epsilon V}(C_1 - C_2) + F_2,$$ (A6)

$$\dot{C}_3 = -\frac{U_{3-4}}{V}(C_4 - C_3),$$ (A7)

$$\dot{C}_4 = -\frac{U_{3-4}}{\epsilon V}(C_6 - C_4),$$ (A8)

$$\dot{C}_5 = -\frac{U_{5-6}}{V}(C_6 - C_5) - \frac{U_{3-4}}{\delta_I V}(C_3 - C_5),$$ (A9)

$$\dot{C}_6 = \frac{\delta_S U_{1-2}}{\epsilon \delta_I V}(C_2 - C_6),$$ (A10)

where C represents either temperature T or the salinity S. The equations for temperature and salinity differ in the forcing terms F_1 and F_2 whose expression is reported in Fig. 1.

The overturning coefficient $\overline{U}_0$ is used as a tuning parameter and is set to the value $\overline{U}_0 = 3.0 \cdot 10^9 \, \text{m}^3 \, \text{s}^{-1} \, \text{m}^3 \, \text{Kg}^{-1}$. Considering the geometrical factors in eqs. (A2)–(A5), this value of $\overline{U}_0$ results into realistic strength of the meridional overturning.

References

Artale, V., Calmanti, S. and Sutera, A. 2003. Thermohaline circulation sensitivity to intermediate level anomalies. *Tellus* **54A**, 159–174.

Bower, A. S., Cann, B. L., Rossby, T., Zenk, W., Gould, J., Speer, K., Richardson, P. L., Prater, M. D. and Zhang, H. M. 2002. Directly measured mid-depth circulation in the northeastern north atlantic. *Nature* **41**, 603–607.

Cessi, P. 1994. A simple box-model of stochastically forced thermohaline flow. *J. Phys. Oceanogr.* **24**, 1911–1920.

Chan, W. and Motoi, T. 2003. Effects of stopping the Mediterranean Outflow on the southern polar region. *Polar Meteorol. Glaciol.* **17**, 25–35.

Curry, R., Dickson, B. and Yashayaev, I. 2003. A change in the freshwater balance of the Atlantic Ocean over the past four decades. *Nature* **426**, 826–829.

Delworth, T. S., Manabe, S. and Stouffer, R. J. 1993. Interdecadal variations of the thermohaline circulation in a coupled ocean-atmosphere model. *J. Climate* **6**, 1993–2011.

Gerdes, R., Köberle, C., Beckmann, A., Herrmann, P. and Willebrand, J. 1999. Mechanisms for spreading of mediterranean water in coarse-resolution numerical models. *J. Phys. Oceanogr.* **29**, 1682–1700.

Griffies, S. M. and Tziperman, E. 1995. A linear thermohaline oscillator driven by stochastic atmospheric forcing. *J. Climate* **8**, 2440–2453.

Lucarini, V. and Stone, P. H. 2005. Thermohaline circulation stability: a box-model study. Part I: uncoupled model. *J. Phys. Oceanogr.* **18**, 501–513.

Marshall, J., Kushnir, Y., Battisti, D., Chang, P., Czaja, A., Dickson, R., Hurrell, J., McCartney, M., Saravanan, R. and Visbeck, M. 2001. North Atlantic climate variability: phenomena, impacts and mechanisms. *Int. J. Climatol.* **21**, 1863–1898.

McCartney, M. and Mauritzen, S. 2001. On the origin of the warm inflow in the Nordic sea. *Progr. in Oceanogr.* **51**, 125–214.

Mikolajewicz, U. and Maier-Reimer, E. 1994. Mixed BCs in ocean general circulation models and their influence on the stability of the model's conveyor belt. *J. Geophys. Res.* **99**, 22 633–22 644.

Potter, R. A. and Lozier, M. S. 2004. On the warming and salinification of the Mediterranean Outflow waters in the North Atlantic. *Geophys. Res. Lett.* **31**, L01202, doi: 10.1029/2003GL018161.

Press, W. H., Teukolsky, S. A., Vetterling, W. T. and Flannery, B. P. 2001. *Numerical Recipes in Fortran 77: The Art of Scientific Computing*, Cambridge University Press, New York, NY.

Rahmstorf, S. 1996. On the freshwater forcing and transport of the Atlantic thermohaline circulation. *Clim. Dyn.* **12**, 799–811.

Rahmstorf, S. 1998. Influence of Mediterranean Outflow on climate. *Eos* **79**, 281–282.

Reid, J. L. 1979. On the contribution of the Mediterranean sea outflow to the Norwegian-Greenland sea. *Deep-Sea Res.* **26**, 1199–1223.

Rivin, I. and Tziperman, E. 1997. Linear versus self sustained interdecadal thermohaline variability in a coupled box-model. *J. Phys. Oceanogr.* **27**, 1216–2446.

Scott, J. R., Marotzke, J. and Stone, P. H. 1999. Interhemispheric thermohaline circulation in a coupled box-model. *J.Phys.Oceanogr.* **29**, 351–365.

Sparrow, M., Boebel, O., Zervakis, V., Cantos-Figuerola, W. Z. A. and Gould, W. J. 2002. Two circulation regimes of the Mediterranean outflow revealed by lagrangian measurements. *J. Phys. Oceanogr.* **32**, 1322–1330.

Stommel, H. 1961. Thermohaline convection with two stable regimes of flow. *Tellus* **13**, 224–227.

Tziperman, E., Toggweiler, R. J., Feliks, Y. and Bryan, K. 1994. Instability of the thermohaline circulation with respect to mixed boundary conditions: Is it really a problem for realistic models? *J. Phys. Ocean.* **24**, 217–232.

Weisse, R., Mikolajevicz, U. and Maier-Reimer, E. 1994. Decadal variability of the north atlantic in an ocean general circulation model. *J. Geophy. Res.* **99**(C6), 12 411–12 421.

Welander, P. 1971. The thermocline problem. *Philos. Trans. Roy. Soc. London* **270A**, 415–421.